

NEAR-INFRARED SPECTROSCOPY OF LOW-MASS KEPLER PLANET-CANDIDATE HOST STARS: EFFECTIVE TEMPERATURES, METALLICITIES, MASSES AND RADII

PHILIP S. MUIRHEAD^{1,2}, KATHERINE HAMREN³, EVERETT SCHLAWIN, BARBARA ROJAS-AYALA⁴, KEVIN R. COVEY⁵, JAMES P. LLOYD

Department of Astronomy, Cornell University, 122 Sciences Drive, Ithaca, NY 14853, USA

(Dated:)

Draft version November 8, 2018

ABSTRACT

We report stellar parameters for low-mass planet-candidate host stars recently announced by the Kepler Mission. We obtained medium-resolution, K-band spectra of 84 low-mass Kepler Objects of Interest (KOIs). We identified one KOI as a giant; for the remaining dwarfs, we estimated effective temperatures (T_{eff}) by comparing measurements of K-band regions dominated by H₂O opacity with predictions of synthetic spectra for low-mass stars. We measured overall metallicities ($[M/H]$) using the equivalent widths of Na I and Ca I absorption features and an empirical metallicity relation calibrated with nearby stars. With effective temperatures and metallicities, we estimate the masses and radii of the low-mass KOIs by interpolation onto evolutionary isochrones. The resultant stellar radii are roughly half of the values reported in the Kepler Input Catalogue and, by construction, correlate better with T_{eff} . Our results significantly reduce the sizes of the corresponding planet-candidates, with many less than 1 Earth radius. Recalculating the equilibrium temperatures of the planet-candidates from the implied stellar luminosities and masses, and assuming Earth's albedo and re-radiation fraction, we find that six of the planet-candidates are terrestrial-sized with orbital semi-major axes that lie within the habitable zones of their low-mass host stars. The stellar parameters presented in this letter serve as a resource for further characterization of the planet-candidates.

Subject headings: Planetary Systems — Stars: fundamental parameters — Stars: abundances — Stars: late-type — Stars: low-mass

1. INTRODUCTION

Estimating physical parameters of stars which host exoplanets is crucial for estimating the physical parameters of the exoplanets themselves. The wealth of detailed information on the Sun has enabled sufficiently precise calibration of stellar evolution models for Sun-like stars that the determination of fundamental stellar physical parameters (mass, effective temperature, luminosity, radius) based on observational atmospheric parameters such as colors and spectra is routine and generally robust (e.g. Kurucz et al. 1984; Kurucz 1991; Nordström et al. 2004; Valenti & Fischer 2005).

For M dwarfs ($T_{\text{eff}} \lesssim 4000$ K, $M \lesssim 0.5 M_{\odot}$), however, the situation is more complex. Low-mass stellar models are not as well calibrated, and differ substantially in predictions depending on assumptions such as mixing length parameter. There are few M dwarfs that are bright enough and nearby enough for accurate parallaxes and direct measurement of radius (e.g. Ségransan et al. 2003; Berger et al. 2006). Eclipsing binaries have been the primary source of radii for M dwarfs, but there has been a longstanding discrepancy between observed radii and

predictions from stellar evolution models (Ribas 2006; Torres 2011). The rapid rotation of close binary systems may be responsible for the discrepancy by inducing magneto-hydrodynamic corrections to the convective efficiency, so these radii may not be representative of field objects (Chabrier et al. 2007; Kraus et al. 2011). Although there remains a monotonic correspondence between spectral type (the observational parameter) and effective temperature, T_{eff} , the calibration of this relationship is not as advanced as it is for solar-type stars. M dwarf atmospheres are fully convective, rich in molecular absorption features and depart substantially from blackbody emission at all wavelengths (Allard et al. 1997), so the empirical effective temperature scale is particularly challenging.

Recently, M dwarfs have received increased attention in both transit and radial velocity searches for exoplanets (e.g. Charbonneau et al. 2009; Bean et al. 2010b; Johnson et al. 2010; Mahadevan et al. 2010; Muirhead et al. 2011), and exoplanet characterization efforts (e.g. Bean et al. 2010a; Désert et al. 2011; Croll et al. 2011), thanks to the higher detectability and characterization signals from orbiting low-mass exoplanets (Nutzman & Charbonneau 2008). In February of 2011 the Kepler Mission announced 997 objects which show light curves consistent with the presence of transiting planets (Borucki et al. 2011), 74 of which have $T_{\text{eff}} < 4400$ K as measured in the Kepler Input Catalog (KIC; Batalha et al. 2010). A statistical analysis of the Kepler Objects of Interest (KOIs) by Howard et al. (2011) reveals a substantial rise in the frequency of short-period, 2-4 R_{\oplus} planets with decreasing T_{eff} of their host stars,

¹ Current address: Department of Astronomy, California Institute of Technology, 1200 East California Boulevard, MC 249-17, Pasadena, CA 91125, USA

² philm@astro.caltech.edu

³ Current address: Department of Astronomy and Astrophysics, University of California Santa Cruz, 1156 High Street, Santa Cruz, CA 95064, USA

⁴ Current address: Astrophysics Department, American Museum of Natural History, Central Park West at 79th Street, New York, NY 10024, USA.

⁵ Hubble Fellow

implying that the low-mass planet candidates detected around low-mass stars represent a ubiquitous population of planets in the galaxy.

Stellar parameters of the KOIs were estimated by the Kepler team as part of the KIC, a photometric survey of stars in the Kepler field-of-view designed to identify bright dwarfs as targets for Kepler. Brown et al. (2011) describes the estimation of physical parameters, whereby the synthetic spectra of Castelli & Kurucz (2004) are forward-modeled—with effective temperature, T_{eff} , surface gravity, $\log(g)$, and metallicity, $\log(Z)$, as free parameters—to match the photometric measurements in the KIC. A relation between luminosity, effective temperature and surface gravity, derived from the stellar evolutionary models computed by Girardi et al. (2000), is used to estimate the stellar masses, which, when combined with $\log(g)$, estimates the radii. Brown et al. (2011) state that the KIC effective temperature and radius estimations are reliable for Sun-like stars, but are “untrustworthy” for stars with T_{eff} less than 3750 K.

Near-infrared spectroscopy offers a more robust method for determining physical parameters of low-mass stars. This is especially true of K-band, spanning roughly from 2.1 to 2.4 μm , as it contains continuum regions sensitive to T_{eff} (Covey et al. 2010), and absorption features that are sensitive to stellar metallicity (Rojas-Ayala et al. 2010), all without being significantly affected by interstellar reddening.

In this letter we present effective temperatures, metallicities, masses and radii of 84 low-mass KOIs from the February 2011 Kepler data release, derived from medium-resolution K-band spectroscopic observations.

2. OBSERVATIONAL CLASSIFICATION

2.1. Observations

Observations were carried out with the TripleSpec Spectrograph at the Palomar Observatory 200-inch Hale Telescope (Herter et al. 2008), a near-infrared slit-spectrograph covering 1.0 to 2.5 μm simultaneously with a resolution of 2700. Two positions on the slit, A and B, were used for each target, and exposures were taken in an ABBA pattern with 60 second integration times at each position. Multiple ABBA sets were taken and combined until each spectrum had a median per-channel signal-to-noise of 60. This was achieved for all of the targets except KOI 51.

For telluric calibration we used SIMBAD to identify a grid of A0 stars in the Kepler field-of-view, and developed an observing sequence such that each KOI observation has a corresponding A0 star observation taken within 40 minutes and with an airmass difference less than 0.1.

2.2. Target Selection

We observed all of the KOIs with KIC-ascribed effective temperatures less than 4400 K over 7 nights in June of 2011. Of the 74 KOIs, 4 appeared to be double objects in the TripleSpec slit viewer with separations of less than 6 arcseconds (roughly the size of the Kepler Spacecraft’s point spread function): KOI 326, KOI 641, KOI 249 and KOI 51, and one consisted of 5 objects within a 6 arcsecond radius: KOI 667. These objects are not included in this letter, except for KOI 51 for which we report observations of the brighter object in the double.

In August of 2011 we observed 15 additional KOIs with KIC-ascribed effective temperatures greater than 4400 K, but with colors indicative of low-mass stars: $(J - K) > 0.7$, $(r - i) > 0.3$, or $(g - r) > 1.0$. We include 13 of these KOIs in this letter, as their spectra revealed CO features indicative of low-mass stars. In total, we obtained spectra of 84 low-mass KOIs.

2.3. Data Analysis

The spectra were extracted using a version of the Spextool program modified for the Palomar TripleSpec Spectrograph (Cushing et al. 2004, ; M. Cushing, private communication 2011). Spextool accepts data in ABBA format. The `xtellcor` package within Spextool accepts spectra of A0 stars and compares them to a model spectrum of Vega to identify and remove telluric absorption lines in a target spectrum (Vacca et al. 2003). Figure 1 plots three example spectra, with templates of similar spectra type and relevant spectral features indicated. The templates are taken from the IRTF Spectral Library (Rayner et al. 2009).

2.4. Spectral Indices

One star in our sample has a K-band spectrum consistent with a giant star, suggesting the observed light curve is due to a stellar, rather than planetary, companion. KOI 977 shows weak Na I and Ca I absorption and strong CO absorption, which qualitatively match IRTF template spectra of giant stars but not dwarf stars of the same spectral type. The spectrum is included in Figure 1, with a giant and dwarf template for comparison.

To estimate the physical parameters of the remaining dwarfs, we measured three spectral indices from the K-band spectra: the equivalent widths of the Na I and Ca I lines, at 2.210 and 2.260 μm respectively, and an index describing the change in flux between three 0.02 μm -wide bands dominated by water opacity—centered at 2.245, 2.370, 2.080 μm —called the H₂O-K2 index. Rojas-Ayala et al. (2011, submitted) describe the measurement of the equivalent widths, introduces H₂O-K2 index, and derives relations between the spectral indices, overall metallicity ($[M/H]$) and KHM spectral type using nearby M dwarfs with F, G or K-type binary companions that have SPOCS $[M/H]$ measurements for calibration (Valenti & Fischer 2005).

3. DETERMINATION OF PHYSICAL PARAMETERS

Since the mass-radius relationship for M dwarfs is reasonably model-independent and the mass-luminosity relationship very steep (see Figure 2), generally the most robust method to estimate the radii of field M dwarfs is to use a measured distance and adopted bolometric corrections to determine the star’s luminosity. The luminosity can then be used with empirical or theoretical mass-luminosity and mass-radius relationships to estimate the mass and radius. Since most KOIs lack distance measurements, it is necessary to estimate masses and radii from effective temperatures and metallicities.

3.1. Effective Temperatures and Metallicities

We used the Rojas-Ayala et al. (2011, submitted) relation to measure the overall metallicity, $[M/H]$, of the KOI targets. For stars identified as K7 by the H₂O-K2

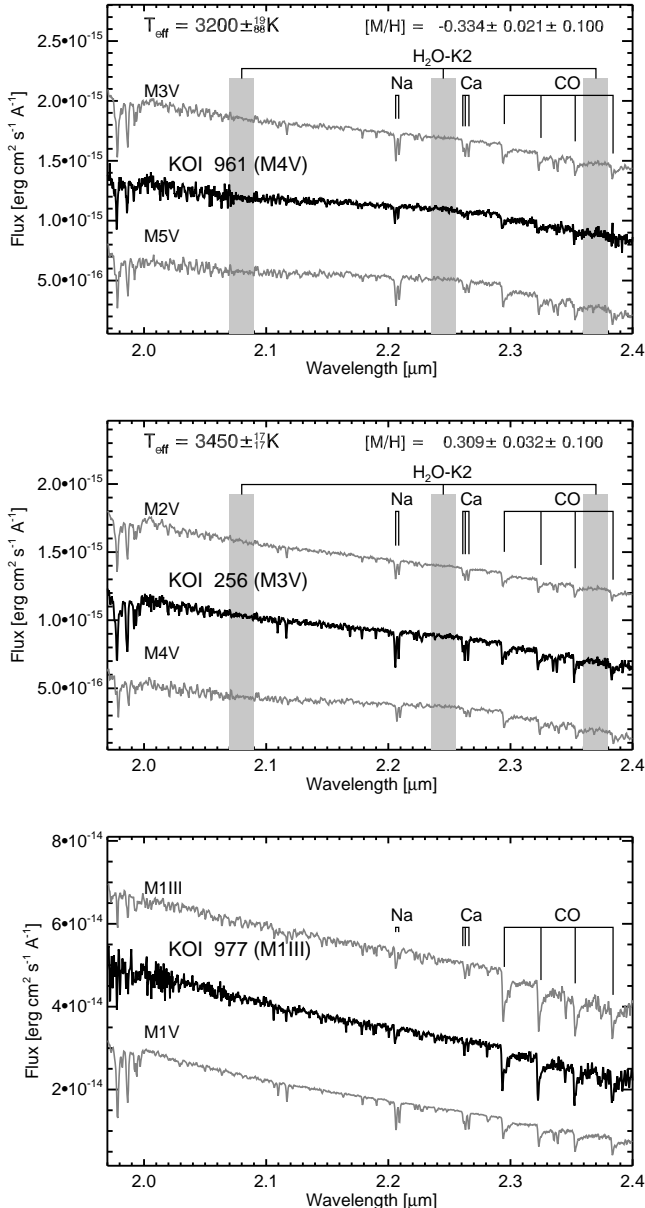


FIG. 1.— TripleSpec K-band spectra of KOIs (black) with comparison KHM spectral type standards from the IRTF Spectral Library (gray, Rayner et al. 2009). The templates are adjusted to the same scale as the KOI spectra using a ratio of the median flux in K band, and then artificially offset. We used the H₂O-K2 index to compute T_{eff} , which is calculated using regions dominated by water opacity, and we used the equivalent widths of the Na I doublet and Ca I triplet to measure $[M/H]$ (Rojas-Ayala et al. 2011, submitted). *Top*: KOI 961 is an example of a metal-poor star with little Na I and Ca I absorption. *Middle*: KOI 256 is an example of a metal-rich star with deep Na I and Ca I absorption. The metallicities $[M/H]$ are included with both random and systematic uncertainties, in that order. *Bottom*: KOI 977 has a spectrum indicative of a giant with deep CO bandheads but relatively weak Na I and Ca I absorption.

index, the $[M/H]$ measurement represents an extrapolation of the M dwarf calibration. The $[M/H]$ of KOI 51 could not be determined because of low signal-to-noise.

To determine T_{eff} , we calculated the H₂O-K2 index on grid of BT-Settl late-type model spectra from Allard et al. (2010) for $3000 \leq T_{\text{eff}} \leq 4400$, $-1 < [M/H] < 0.5$, and $\log(g)=5.0$, creating a surface of T_{eff} as a func-

tion of H₂O-K2 and $[M/H]$. For each KOI, we interpolated the measured H₂O-K2 and $[M/H]$ values onto the surface. The T_{eff} surface is very metallicity insensitive ($< 10\text{K}$ offsets due to metallicity effects) for $3200 < T_{\text{eff}} < 3900$, and $[M/H] < 0.3$. For higher temperatures the H₂O-K2 index saturates, where the saturation T_{eff} depends on $[M/H]$. The saturation introduces metallicity offsets for $T_{\text{eff}} > 3900\text{K}$, and for super metal-rich stars ($[M/H] > 0.3$) at $T_{\text{eff}} > 3700\text{K}$.

3.2. Stellar Masses and Radii

For the purposes of this paper, we place the low-mass KOIs on a grid of physical parameters based on the Padova stellar evolution models (Girardi et al. 2002). These models are in generally good agreement with observations, but there may well be systematic offsets in mass, radius or effective temperature, so these inferred physical parameters should be used with caution.

All but two of the stars are treated homogeneously, so the relative radii, masses and temperatures should be precise, even in the presence of model-dependent offsets. There is no model in the Girardi et al. (2002) isochrones with the same metallicity and effective temperature as KOI 961 or 249, so these stars are placed on a 5-Gyr isochrone from the Baraffe et al. (1998) models.

Stellar masses and radii are calculated by interpolation of the main sequence of a 5-Gyr isochrone at the measured total metallicity and effective temperature, illustrated in Figures 3 and 4. The assumption of age does not significantly change the results. If very young ages are adopted, the masses and radii typically change only 0.1% between ages of 1 and 10 Gyr, and in all cases significantly less than the reported uncertainties.

4. ERROR ANALYSIS

We estimate the uncertainty in the equivalent width, H₂O-K2 index and $[M/H]$ measurements due to noise in the spectra using Monte Carlo simulations. Spextool reports errors for each channel of a reduced spectrum assuming photon noise and read noise in the target and telluric calibrator exposures. For each reduced spectrum, we created 1000 copies, each with random noise added to the spectral channels based on the error reported by Spextool. For each of the 1000 simulations, we measure the equivalent widths, H₂O-K2 index and calculate $[M/H]$ from them. The standard deviations of the quantities across the simulations are taken as the *random* uncertainty in those quantities for a given KOI.

The $[M/H]$ estimate contains additional uncertainty from the calibration relation. Possible sources of calibration errors include astrophysical scatter from non-perfect correlation between the indices and $[M/H]$, as well as errors in the relation coefficients due to noise in the calibration spectra. Rojas-Ayala et al. (2011, submitted) estimates the calibration errors contribute 0.1 dex of error to $[M/H]$ measurements, based on the root-mean-square residuals in the calibration fit. We distinguish between *random* errors (stemming from the noise in the spectra) and *systematic* errors (resulting from the calibration itself), because the systematic errors likely affect all measurements in a similar manner. We propagate both independently to the stellar mass and radius.

The observational uncertainty in T_{eff} is propagated by repeating the calculation for H₂O-K2 indices which are

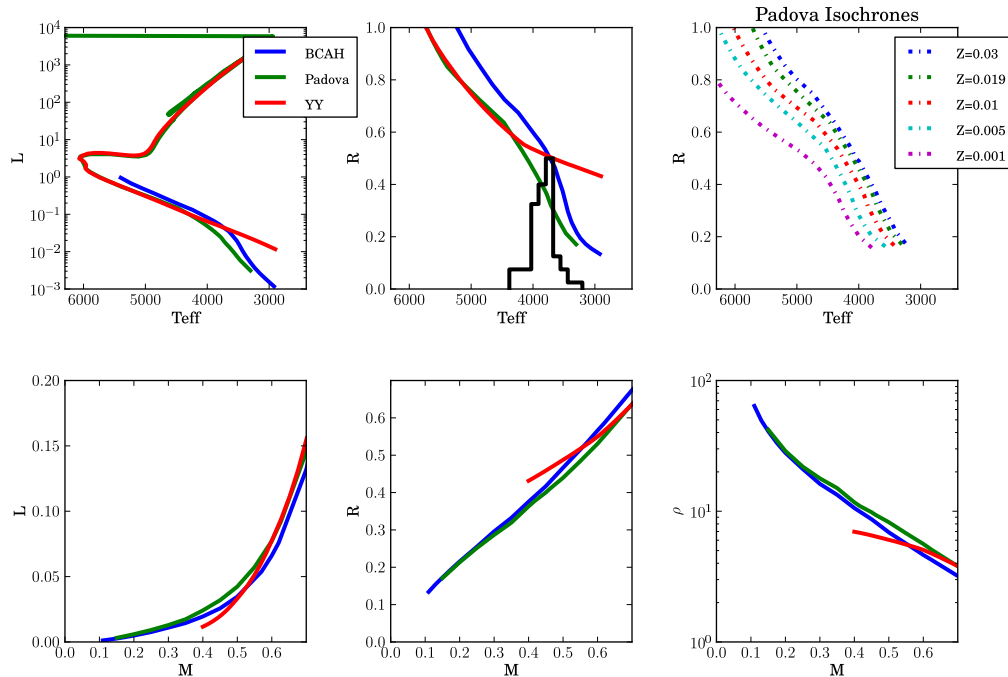


FIG. 2.— Comparison between 5-Gyr isochrones for stellar evolution models. In the top left panel is a conventional theoretical Hertzsprung-Russell diagram (T_{eff} vs L) for three sets of solar metallicity isochrones: Yonsei-Yale (Yi et al. 2003), Padova (Girardi et al. 2002) and BCAH98 (Baraffe et al. 1998). In the top center panel is shown the relationship between radius and effective temperature for all three solar metallicity models and a histogram of the effective temperatures for the sample reported in this paper. The Yonsei-Yale and Padova isochrones are in good agreement for $T_{\text{eff}} > 4500$ K, but there are major differences between all three models for $T_{\text{eff}} < 4500$ K. The BCAH isochrones do not agree with conventional models for solar-type stars because they adopt a mixing length parameter $\alpha = H_P/l_{\text{mix}}$ of 1.0, as opposed to the solar-calibrated value of 1.7. The top right shows the effect of varying metallicity on the radius. The lower panels show the relationships between stellar mass, luminosity, radius and density respectively.

1- σ higher and lower than the measured value. Since the $\text{H}_2\text{O-K2}$ index begins to saturate at $3700 T_{\text{eff}}$, the errors for T_{eff} near and above this value are asymmetric. For several M0V and K7V KOIs, the uncertainties based on the $\text{H}_2\text{O} - \text{K}$ index were unreasonably large, so these stars were assigned $T_{\text{eff}} = 4000 \pm 200$ K and $T_{\text{eff}} = 4400 \pm 200$ K based on their spectral types of M0V and K7V, respectively.

The asymmetric errors in T_{eff} and the random and systematic uncertainties in $[\text{M}/\text{H}]$ are propagated to mass and radius using Monte-Carlo simulations. Figure 3 plots an example KOI including the results from Monte-Carlo simulations of noise in T_{eff} and $[\text{M}/\text{H}]$. The distribution of resultant stellar masses and radii is relatively symmetric, despite the asymmetric T_{eff} errors. We therefore quote the random and systematic uncertainties in mass and radius as a single 1- σ value.

5. RESULTS AND DISCUSSION

Table 1 lists the KOI planet candidates and our measurements of their host star parameters: spectral type, effective temperature, metallicity, and mass and radius, with random and systematic errors listed separately. We also include our estimate of the planet candidate radii, calculated by scaling the planet radius reported in Borucki et al. (2011) by the ratio of our stellar radius to the value in the KIC. It should be noted that the appropriate limb-darkening coefficient could change as a

result of the stellar classification, requiring a more sophisticated calculation of the new planet-candidate radii than in this letter.

Figure 4 plots the effective temperatures, metallicities and resultant radii from our analysis as well as the values in the KIC. Our stellar radii are systematically lower than the values reported in the KIC by roughly a factor of two and, by construction, have better agreement with T_{eff} . The smaller stellar radii imply smaller planet-candidate radii, and many of the revised planet-candidate radii are smaller than 1 Earth radius.

Interestingly, the metallicity distribution of the low-mass KOIs in our sample is metal-poor, with a median $[\text{M}/\text{H}]$ of -0.10 and a standard deviation of 0.16. At first this would appear contradictory to the planet-metallicity correlation (e.g. Santos et al. 2001; Fischer & Valenti 2005), which has been extended to M dwarfs (Johnson & Apps 2009; Schlaufman & Laughlin 2010; Rojas-Ayala et al. 2010). However, exoplanets which transit metal-poor M-dwarfs have higher detectability with Kepler because the stars are both bluer and smaller than metal-rich M dwarfs of the same luminosity. Being bluer, they have more flux in the visible-wavelengths and are likely more common in the Kepler target list, which is magnitude-limited subsample of the KIC. Being smaller, a transiting planet has a relatively deeper transit light curve and is therefore more detectable. The Kepler field-of-view is also located $\sim 10^\circ$

KOI 247 (M1V) Mass/Radius Monte Carlo (5 Gyr Isochrone)

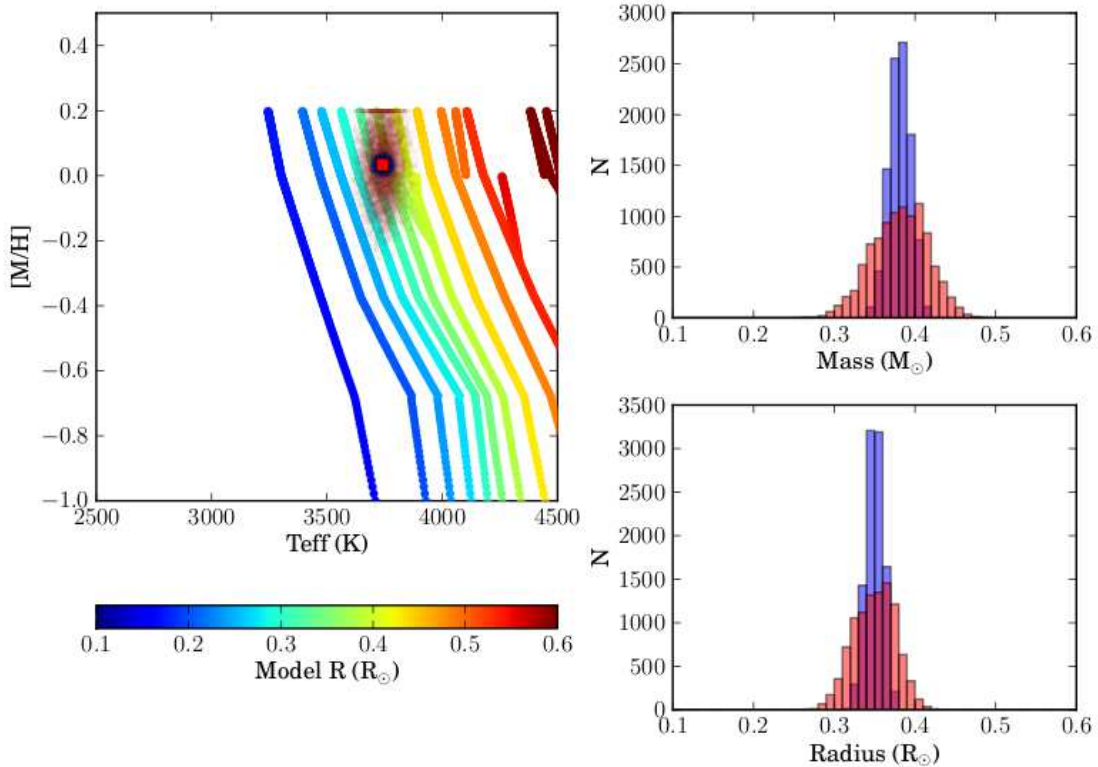


FIG. 3.— Plots showing the determination of mass, radius and corresponding uncertainties for a KOI 247, a typical object in our sample. *Left*: 5-Gyr Padova isochrones versus $[M/H]$, T_{eff} and R_{\odot} , and the interpolated location of KOI 247. For each KOI in our sample we measure T_{eff} and $[M/H]$ from the K-band spectra, and interpolate the mass and radius using the isochrone grid. We include the Monte-Carlo simulations of noise in $[M/H]$ and T_{eff} , which appear as a cloud of points. The blue points assume only random noise in the $[M/H]$ and T_{eff} stemming from noise in the spectrum. The red points use the systematic errors of 0.1 dex and 125 K, respectively. The Padova isochrones do not include $[M/H]$ greater than 0.2, so we assign all Monte-Carlo simulations with a value higher than this to 0.2. *Right*: Monte Carlo results for interpolated stellar mass (*top*) and radius (*bottom*). We quote the standard deviation in mass and radius for assuming both random and systematic errors in Table 1.

off the galactic plane, and likely contains many metal-poor thick disk stars. Schlaufman & Laughlin (2011) used the KIC-photometry to infer metallicities and found the low-mass KOIs are systematically metal-rich compared to a random sample of Kepler targets without planetary transits. Our results are not inconsistent if the Kepler target list is itself biased toward metal-poor M dwarfs.

The effective temperatures, radii and masses of the KOIs imply different planet-candidate equilibrium temperature estimates, such that 6 planet-candidates are terrestrial-sized and have equilibrium temperatures which may permit liquid water to reside on the planet surface, assuming Earth-like albedos and re-radiation fractions. Scaling the Earth’s equilibrium temperature of 255 K by the orbital semi-major axis, stellar T_{eff} and stellar radius of the KOIs in this letter, we find that KOIs 463.01, 1422.02, 947.01, 812.03, 448.02 and 1361.01 all have equilibrium temperatures between 217 K and 261 K: the limits of the habitable zone as described in Kasting et al. (1993). This assumes the same albedo, re-radiation fraction and greenhouse effect as the Earth-Sun system: a naive assumption for terrestrial planets orbiting M dwarfs. While the question of whether liquid

water can persist on the surfaces of planet candidates orbiting low-mass stars depends strongly on the individual evolution and atmospheric peculiarities of each system (e.g. Tarter et al. 2007), these KOIs are nevertheless compelling targets for future followup work.

A recent paper by Gaidos et al. (2011) compares the statistics from the M2K M-dwarf Doppler survey (e.g. Apps et al. 2010) with the Kepler results. They found inconsistencies which could be explained if many of the KOI stellar radii were underestimated: a result which is contradictory to our findings. However, the KIC T_{eff} used to compare the M2K and Kepler samples differ from our measurements, and the two samples have very different metallicity distributions.

We would like to thank Michael Cushing for providing us with a version of the Spextool package for the Triple-Spec Spectrograph at Palomar. We would also like to thank John Johnson for his thoughtful comments on the letter. The Palomar 200-inch Telescope time was provided by Cornell University.

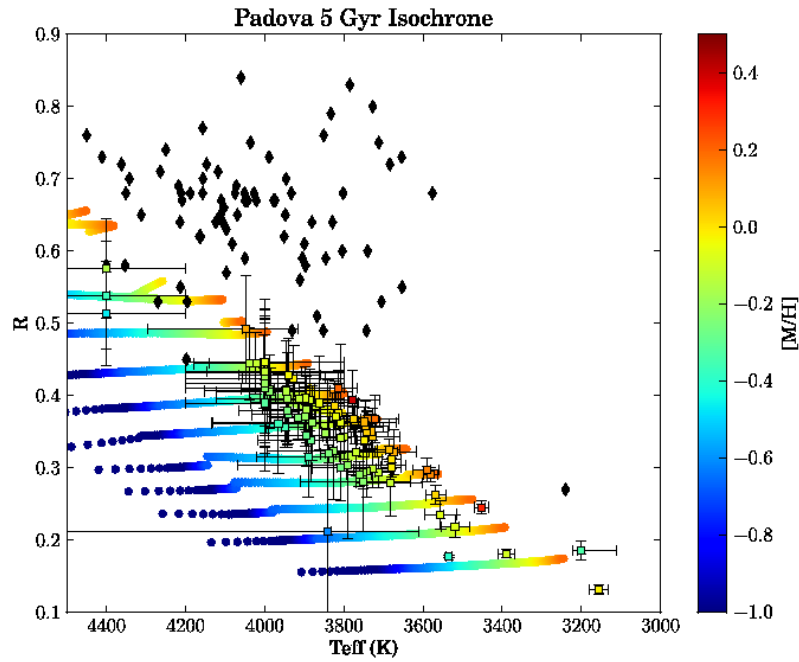


FIG. 4.— Temperature, metallicity and radius determinations for our sample of low-mass KOIs. Squares with errorbars are the measurements in this paper, black diamonds are the values from the KIC, and the circles/tracks are 5-Gyr isochrones from Girardi et al. (2002). Since $Z=0.03$ ($[M/H]=0.2$) is the maximum metallicity in the Girardi et al. (2002) isochrones, the $Z=0.03$ isochrone has been used for the more metal-rich stars. For the stars that are cooler than anything in the Girardi et al. (2002) isochrones, KOIs 961 and 249, the Baraffe et al. (1998) solar-metallicity isochrone has been used. Since KOI 961 is metal poor, its radius is likely over-estimated by the Baraffe et al. (1998) models.

REFERENCES

- Allard, F., Hauschildt, P. H., Alexander, D. R., & Starrfield, S. 1997, *ARA&A*, 35, 137
- Allard, F., Homeier, D., & Freytag, B. 2010, *ArXiv e-prints*
- Apps, K., Clubb, K. I., Fischer, D. A., Gaidos, E., Howard, A., Johnson, J. A., Marcy, G. W., Isaacson, H., Giguere, M. J., Valenti, J. A., Rodriguez, V., Chubak, C., & Lepine, S. 2010, *PASP*, 122, 156
- Baraffe, I., Chabrier, G., Allard, F., & Hauschildt, P. H. 1998, *A&A*, 337, 403
- Batalha, N. M., Borucki, W. J., Koch, D. G., Bryson, S. T., Haas, M. R., Brown, T. M., Caldwell, D. A., Hall, J. R., Gilliland, R. L., Latham, D. W., Meibom, S., & Monet, D. G. 2010, *ApJ*, 713, L109
- Bean, J. L., Miller-Ricci Kempton, E., & Homeier, D. 2010a, *Nature*, 468, 669
- Bean, J. L., Seifahrt, A., Hartman, H., Nilsson, H., Wiedemann, G., Reiners, A., Dreizler, S., & Henry, T. J. 2010b, *ApJ*, 713, 410
- Berger, D. H., Gies, D. R., McAlister, H. A., ten Brummelaar, T. A., Henry, T. J., Sturmman, J., Sturmman, L., Turner, N. H., Ridgway, S. T., Aufdenberg, J. P., & Mérand, A. 2006, *ApJ*, 644, 475
- Borucki, W. J., Koch, D. G., Basri, G., Batalha, N., Brown, T. M., Bryson, S. T., Caldwell, D., Christensen-Dalsgaard, J., Cochran, W. D., DeVore, E., Dunham, E. W., Gautier, III, T. N., Geary, J. C., Gilliland, R., Gould, A., Howell, S. B., Jenkins, J. M., Latham, D. W., Lissauer, J. J., Marcy, G. W., Rowe, J., Sasselov, D., Boss, A., Charbonneau, D., Ciardi, D., Doyle, L., Dupree, A. K., Ford, E. B., Fortney, J., Holman, M. J., Seager, S., Steffen, J. H., Tarter, J., Welsh, W. F., Allen, C., Buchhave, L. A., Christiansen, J. L., Clarke, B. D., Désert, J.-M., Endl, M., Fabrycky, D., Fressin, F., Haas, M., Horch, E., Howard, A., Isaacson, H., Kjeldsen, H., Kolodziejczak, J., Kulesa, C., Li, J., Machalek, P., McCarthy, D., MacQueen, P., Meibom, S., Miquel, T., Prsa, A., Quinn, S. N., Quintana, E. V., Ragozzine, D., Sherry, W., Shporer, A., Tenenbaum, P., Torres, G., Twicken, J. D., Van Cleve, J., & Walkowicz, L. 2011, *ArXiv e-prints*
- Brown, T. M., Latham, D. W., Everett, M. E., & Esquerdo, G. A. 2011, *ArXiv e-prints*
- Castelli, F. & Kurucz, R. L. 2004, *ArXiv Astrophysics e-prints*
- Chabrier, G., Gallardo, J., & Baraffe, I. 2007, *A&A*, 472, L17
- Charbonneau, D., Berta, Z. K., Irwin, J., Burke, C. J., Nutzman, P., Buchhave, L. A., Lovis, C., Bonfils, X., Latham, D. W., Udry, S., Murray-Clay, R. A., Holman, M. J., Falco, E. E., Winn, J. N., Queloz, D., Pepe, F., Mayor, M., Delfosse, X., & Forveille, T. 2009, *Nature*, 462, 891
- Covey, K. R., Lada, C. J., Román-Zúñiga, C., Muench, A. A., Forbrich, J., & Ascenso, J. 2010, *ApJ*, 722, 971
- Croll, B., Albert, L., Jayawardhana, R., Miller-Ricci Kempton, E., Fortney, J. J., Murray, N., & Neilson, H. 2011, *ApJ*, 736, 78
- Cushing, M. C., Vacca, W. D., & Rayner, J. T. 2004, *PASP*, 116, 362
- Désert, J.-M., Bean, J., Miller-Ricci Kempton, E., Berta, Z. K., Charbonneau, D., Irwin, J., Fortney, J., Burke, C. J., & Nutzman, P. 2011, *ApJ*, 731, L40+
- Fischer, D. A. & Valenti, J. 2005, *ApJ*, 622, 1102
- Gaidos, E., Fischer, D. A., Mann, A. W., & Lepine, S. 2011, *ArXiv e-prints*
- Girardi, L., Bertelli, G., Bressan, A., Chiosi, C., Groenewegen, M. A. T., Marigo, P., Salasnich, B., & Weiss, A. 2002, *A&A*, 391, 195
- Girardi, L., Bressan, A., Bertelli, G., & Chiosi, C. 2000, *A&AS*, 141, 371
- Herter, T. L., Henderson, C. P., Wilson, J. C., Matthews, K. Y., Rahmer, G., Bonati, M., Muirhead, P. S., Adams, J. D., Lloyd, J. P., Skrutskie, M. F., Moon, D., Parshley, S. C., Nelson, M. J., Martinache, F., & Gull, G. E. 2008, in *Society of Photo-Optical Instrumentation Engineers (SPIE) Conference Series*, Vol. 7014, Society of Photo-Optical Instrumentation Engineers (SPIE) Conference Series
- Howard, A. W., Marcy, G. W., Bryson, S. T., Jenkins, J. M., Rowe, J. F., Batalha, N. M., Borucki, W. J., Koch, D. G., Dunham, E. W., Gautier, III, T. N., Van Cleve, J., Cochran, W. D., Latham, D. W., Lissauer, J. J., Torres, G., Brown, T. M., Gilliland, R. L., Buchhave, L. A., Caldwell, D. A., Christensen-Dalsgaard, J., Ciardi, D., Fressin, F., Haas, M. R., Howell, S. B., Kjeldsen, H., Seager, S., Rogers, L., Sasselov, D. D., Steffen, J. H., Basri, G. S., Charbonneau, D., Christiansen, J., Clarke, B., Dupree, A., Fabrycky, D. C., Fischer, D. A., Ford, E. B., Fortney, J. J., Tarter, J., Girouard, F. R., Holman, M. J., Johnson, J. A., Klaus, T. C., Machalek, P., Moorhead, A. V., Morehead, R. C., Ragozzine, D., Tenenbaum, P., Twicken, J. D., Quinn, S. N., Isaacson, H., Shporer, A., Lucas, P. W., Walkowicz, L. M., Welsh, W. F., Boss, A., Devore, E., Gould, A., Smith, J. C., Morris, R. L., Prsa, A., & Morton, T. D. 2011, *ArXiv e-prints*
- Johnson, J. A., Aller, K. M., Howard, A. W., & Crepp, J. R. 2010, *PASP*, 122, 905
- Johnson, J. A. & Apps, K. 2009, *ApJ*, 699, 933
- Kasting, J. F., Whitmire, D. P., & Reynolds, R. T. 1993, *Icarus*, 101, 108
- Kraus, A. L., Tucker, R. A., Thompson, M. I., Craine, E. R., & Hillenbrand, L. A. 2011, *ApJ*, 728, 48
- Kurucz, R. L. The solar spectrum, ed. Cox, A. N., Livingston, W. C., & Matthews, M. S., 663–669
- Kurucz, R. L., Furenlid, I., Brault, J., & Testerman, L. 1984, *Solar flux atlas from 296 to 1300 nm*, ed. Kurucz, R. L., Furenlid, I., Brault, J., & Testerman, L.
- Mahadevan, S., Ramsey, L., Wright, J., Endl, M., Redman, S., Bender, C., Roy, A., Zonak, S., Troupe, N., Engel, L., Sigurdsson, S., Wolszczan, A., & Zhao, B. 2010, in *Society of Photo-Optical Instrumentation Engineers (SPIE) Conference Series*, Vol. 7735, Society of Photo-Optical Instrumentation Engineers (SPIE) Conference Series
- Muirhead, P. S., Edelstein, J., Erskine, D. J., Wright, J. T., Muterspaugh, M. W., Covey, K. R., Wishnow, E. H., Hamren, K., Andelson, P., Kimber, D., Mercer, T., Halverson, S. P., Vanderburg, A., Mondo, D., Czeszumaska, A., & Lloyd, J. P. 2011, *PASP*, 123, 709
- Nordström, B., Mayor, M., Andersen, J., Holmberg, J., Pont, F., Jørgensen, B. R., Olsen, E. H., Udry, S., & Mowlavi, N. 2004, *A&A*, 418, 989
- Nutzman, P. & Charbonneau, D. 2008, *PASP*, 120, 317
- Rayner, J. T., Cushing, M. C., & Vacca, W. D. 2009, *ApJS*, 185, 289
- Ribas, I. 2006, *Ap&SS*, 304, 89
- Rojas-Ayala, B., Covey, K. R., Muirhead, P. S., & Lloyd, J. P. 2010, *ApJ*, 720, L113
- . 2011, submitted
- Santos, N. C., Israelian, G., & Mayor, M. 2001, *A&A*, 373, 1019
- Schlaufman, K. C. & Laughlin, G. 2010, *A&A*, 519, A105+
- . 2011, *ArXiv e-prints*
- Ségransan, D., Kervella, P., Forveille, T., & Queloz, D. 2003, *A&A*, 397, L5
- Tarter, J. C., Backus, P. R., Mancinelli, R. L., Aurnou, J. M., Backman, D. E., Basri, G. S., Boss, A. P., Clarke, A., Deming, D., Doyle, L. R., Feigelson, E. D., Freund, F., Grinspoon, D. H., Haberle, R. M., Hauck, II, S. A., Heath, M. J., Henry, T. J., Hollingsworth, J. L., Joshi, M. M., Kilston, S., Liu, M. C., Meikle, E., Reid, I. N., Rothschild, L. J., Scalo, J., Segura, A., Tang, C. M., Tiedje, J. M., Turnbull, M. C., Walkowicz, L. M., Weber, A. L., & Young, R. E. 2007, *Astrobiology*, 7, 30
- Torres, G. 2011, *ArXiv e-prints*
- Vacca, W. D., Cushing, M. C., & Rayner, J. T. 2003, *PASP*, 115, 389
- Valenti, J. A. & Fischer, D. A. 2005, *ApJS*, 159, 141
- Yi, S. K., Kim, Y.-C., & Demarque, P. 2003, *ApJS*, 144, 259

TABLE 1
LATE-TYPE KOI HOST AND PLANET PROPERTIES

KOI	Sp Type	[M/H] $\pm \sigma_{\text{Ran}} \pm \sigma_{\text{Sys}}$	$T_{\text{eff}} \pm \sigma_{\text{Ran}} \pm \sigma_{\text{Sys}}$ [K]	$M_* \pm \sigma_{\text{Ran}} \pm \sigma_{\text{Sys}}$ [M_{\odot}]	$R_* \pm \sigma_{\text{Ran}} \pm \sigma_{\text{Sys}}$ [R_{\odot}]	$R_{\text{P}} \pm \sigma_{\text{Ran}} \pm \sigma_{\text{Sys}}$ [R_{\oplus}]	$T_{\text{eq}} \pm \sigma_{\text{Sys}}$ [K]
961.01	M4V	-0.33 \pm 0.02 \pm 0.10	3200 ⁺²⁰ ₋₉₀ \pm 50	0.16 \pm 0.01 \pm 0.02	0.19 \pm 0.01 \pm 0.01	1.06 \pm 0.07 \pm 0.08	550 \pm 39
961.02	3.92 \pm 0.27 \pm 0.30	764 \pm 55
961.03	2.92 \pm 0.20 \pm 0.22	476 \pm 34
463.01	M3V	-0.09 \pm 0.02 \pm 0.10	3389 ⁺²¹ ₋₂₂ \pm 50	0.16 \pm 0.01 \pm 0.02	0.18 \pm 0.01 \pm 0.01	0.93 \pm 0.03 \pm 0.07	232 \pm 15
256.01	M3V	0.31 \pm 0.02 \pm 0.10	3452 ⁺¹⁸ ₋₁₈ \pm 50	0.24 \pm 0.01 \pm 0.03	0.25 \pm 0.01 \pm 0.02	3.30 \pm 0.12 \pm 0.29	616 \pm 49
1422.01	M2V	-0.07 \pm 0.04 \pm 0.10	3519 ⁺³⁵ ₋₃₇ \pm 50	0.21 \pm 0.02 \pm 0.03	0.22 \pm 0.02 \pm 0.02	0.91 \pm 0.06 \pm 0.08	374 \pm 30
1422.02	0.85 \pm 0.06 \pm 0.08	249 \pm 20
1422.03	0.58 \pm 0.04 \pm 0.05	439 \pm 36
1146.01	M2V	-0.07 \pm 0.05 \pm 0.10	3555 ⁺⁴⁰ ₋₄₁ \pm 50	0.23 \pm 0.03 \pm 0.03	0.24 \pm 0.02 \pm 0.02	0.60 \pm 0.05 \pm 0.06	361 \pm 30
899.01	M2V	0.02 \pm 0.03 \pm 0.10	3567 ⁺²⁴ ₋₂₄ \pm 50	0.26 \pm 0.02 \pm 0.03	0.26 \pm 0.01 \pm 0.02	0.81 \pm 0.04 \pm 0.07	374 \pm 30
899.02	0.62 \pm 0.03 \pm 0.06	483 \pm 39
899.03	0.81 \pm 0.04 \pm 0.07	289 \pm 23
936.01	M2V	0.14 \pm 0.02 \pm 0.10	3580 ⁺¹⁹ ₋₁₈ \pm 50	0.30 \pm 0.01 \pm 0.03	0.29 \pm 0.01 \pm 0.02	1.41 \pm 0.04 \pm 0.11	352 \pm 25
936.02	0.81 \pm 0.03 \pm 0.06	773 \pm 55
854.01	M2V	0.16 \pm 0.04 \pm 0.10	3591 ⁺³⁴ ₋₃₁ \pm 50	0.31 \pm 0.02 \pm 0.03	0.30 \pm 0.02 \pm 0.02	1.15 \pm 0.06 \pm 0.09	196 \pm 14
781.01	M1V	0.09 \pm 0.06 \pm 0.10	3673 ⁺⁶¹ ₋₅₆ \pm 50	0.35 \pm 0.04 \pm 0.04	0.32 \pm 0.03 \pm 0.03	1.76 \pm 0.17 \pm 0.15	347 \pm 26
736.01	M1V	-0.11 \pm 0.10 \pm 0.10	3681 ⁺⁸⁸ ₋₇₉ \pm 50	0.29 \pm 0.06 \pm 0.04	0.28 \pm 0.05 \pm 0.03	1.07 \pm 0.17 \pm 0.13	283 \pm 28
736.02	0.82 \pm 0.13 \pm 0.10	398 \pm 40
610.01	M1V	-0.02 \pm 0.02 \pm 0.10	3680 ⁺²⁴ ₋₂₄ \pm 50	0.32 \pm 0.02 \pm 0.03	0.30 \pm 0.01 \pm 0.03	0.87 \pm 0.04 \pm 0.07	317 \pm 24
596.01	M1V	0.00 \pm 0.02 \pm 0.10	3679 ⁺²³ ₋₂₃ \pm 50	0.33 \pm 0.02 \pm 0.04	0.31 \pm 0.01 \pm 0.03	0.88 \pm 0.04 \pm 0.07	655 \pm 49
1164.01	M1V	0.07 \pm 0.03 \pm 0.10	3686 ⁺²⁸ ₋₂₆ \pm 50	0.35 \pm 0.02 \pm 0.03	0.32 \pm 0.02 \pm 0.03	0.51 \pm 0.02 \pm 0.04	560 \pm 39
1201.01	M1V	-0.11 \pm 0.05 \pm 0.10	3713 ⁺³⁹ ₋₃₇ \pm 50	0.31 \pm 0.03 \pm 0.04	0.29 \pm 0.02 \pm 0.03	0.84 \pm 0.06 \pm 0.08	549 \pm 45
818.01	M1V	0.19 \pm 0.08 \pm 0.10	3720 ⁺⁷¹ ₋₅₉ \pm 50	0.40 \pm 0.04 \pm 0.03	0.37 \pm 0.03 \pm 0.03	1.59 \pm 0.14 \pm 0.11	412 \pm 26
886.01	M1V	-0.12 \pm 0.05 \pm 0.10	3727 ⁺⁴⁵ ₋₄₅ \pm 50	0.32 \pm 0.04 \pm 0.04	0.30 \pm 0.03 \pm 0.03	1.13 \pm 0.10 \pm 0.11	387 \pm 32
952.01	M1V	0.04 \pm 0.08 \pm 0.10	3726 ⁺⁷³ ₋₆₇ \pm 50	0.37 \pm 0.05 \pm 0.04	0.34 \pm 0.04 \pm 0.03	1.41 \pm 0.16 \pm 0.13	449 \pm 35
952.02	1.41 \pm 0.16 \pm 0.13	393 \pm 31
952.03	1.47 \pm 0.17 \pm 0.14	286 \pm 22
952.04	0.67 \pm 0.08 \pm 0.06	569 \pm 45
739.01	M1V	0.07 \pm 0.04 \pm 0.10	3731 ⁺⁴⁵ ₋₄₃ \pm 50	0.38 \pm 0.03 \pm 0.04	0.35 \pm 0.02 \pm 0.03	1.05 \pm 0.07 \pm 0.08	752 \pm 51
778.01	M1V	-0.16 \pm 0.06 \pm 0.10	3742 ⁺⁶⁷ ₋₆₃ \pm 50	0.32 \pm 0.05 \pm 0.04	0.30 \pm 0.04 \pm 0.03	0.92 \pm 0.11 \pm 0.09	593 \pm 51
1404.01	M1V	-0.23 \pm 0.11 \pm 0.10	3751 ⁺¹⁵⁹ ₋₁₁₈ \pm 50	0.30 \pm 0.09 \pm 0.05	0.28 \pm 0.07 \pm 0.04	0.73 \pm 0.18 \pm 0.10	408 \pm 45
478.01	M1V	0.13 \pm 0.01 \pm 0.10	3740 ⁺¹⁷ ₋₁₇ \pm 50	0.40 \pm 0.01 \pm 0.03	0.37 \pm 0.01 \pm 0.02	2.07 \pm 0.05 \pm 0.14	374 \pm 22
252.01	M1V	0.06 \pm 0.04 \pm 0.10	3742 ⁺⁴² ₋₄₂ \pm 50	0.39 \pm 0.03 \pm 0.04	0.36 \pm 0.02 \pm 0.03	1.66 \pm 0.11 \pm 0.13	317 \pm 21
947.01	M1V	-0.18 \pm 0.04 \pm 0.10	3751 ⁺⁴¹ ₋₄₀ \pm 50	0.32 \pm 0.03 \pm 0.04	0.29 \pm 0.02 \pm 0.03	1.24 \pm 0.09 \pm 0.11	254 \pm 20
247.01	M1V	0.03 \pm 0.01 \pm 0.10	3742 ⁺¹⁶ ₋₁₆ \pm 50	0.38 \pm 0.01 \pm 0.03	0.35 \pm 0.01 \pm 0.03	1.23 \pm 0.03 \pm 0.09	341 \pm 23
1459.01	M1V	0.07 \pm 0.07 \pm 0.10	3745 ⁺⁶⁴ ₋₅₉ \pm 50	0.39 \pm 0.04 \pm 0.04	0.36 \pm 0.03 \pm 0.03	2.95 \pm 0.28 \pm 0.25	935 \pm 69
817.01	M1V	0.08 \pm 0.03 \pm 0.10	3749 ⁺⁴¹ ₋₄₁ \pm 50	0.40 \pm 0.03 \pm 0.03	0.36 \pm 0.02 \pm 0.03	1.29 \pm 0.08 \pm 0.09	288 \pm 18
227.01	M1V	-0.02 \pm 0.02 \pm 0.10	3747 ⁺²⁰ ₋₂₀ \pm 50	0.37 \pm 0.02 \pm 0.04	0.34 \pm 0.01 \pm 0.04	1.46 \pm 0.06 \pm 0.16	311 \pm 27
253.01	M1V	0.40 \pm 0.08 \pm 0.10	3778 ⁺¹¹³ ₋₆₉ \pm 50	0.44 \pm 0.05 \pm 0.03	0.39 \pm 0.04 \pm 0.02	1.85 \pm 0.19 \pm 0.11	463 \pm 25
571.01	M1V	-0.21 \pm 0.04 \pm 0.10	3761 ⁺³¹ ₋₃₀ \pm 50	0.31 \pm 0.02 \pm 0.04	0.29 \pm 0.02 \pm 0.03	0.77 \pm 0.05 \pm 0.07	401 \pm 32
571.02	0.91 \pm 0.05 \pm 0.08	327 \pm 26
571.03	0.82 \pm 0.05 \pm 0.07	494 \pm 39
784.01	M1V	-0.10 \pm 0.04 \pm 0.10	3768 ⁺⁶¹ ₋₅₃ \pm 50	0.36 \pm 0.04 \pm 0.04	0.32 \pm 0.03 \pm 0.03	1.14 \pm 0.12 \pm 0.10	299 \pm 23
255.01	M1V	0.02 \pm 0.04 \pm 0.10	3771 ⁺⁶⁶ ₋₅₄ \pm 50	0.40 \pm 0.04 \pm 0.04	0.36 \pm 0.03 \pm 0.03	1.80 \pm 0.16 \pm 0.17	277 \pm 21
1026.01	M1V	0.03 \pm 0.03 \pm 0.10	3775 ⁺³¹ ₋₂₉ \pm 50	0.40 \pm 0.02 \pm 0.04	0.37 \pm 0.02 \pm 0.03	0.97 \pm 0.04 \pm 0.09	184 \pm 14
494.01	M1V	-0.21 \pm 0.14 \pm 0.10	3790 ⁺²⁷⁸ ₋₁₄₆ \pm 50	0.33 \pm 0.13 \pm 0.06	0.30 \pm 0.10 \pm 0.04	1.05 \pm 0.35 \pm 0.15	268 \pm 31

TABLE 1 — *Continued*

KOI	Sp Type	[M/H] $\pm \sigma_{\text{Ran}} \pm \sigma_{\text{Sys}}$	$T_{\text{eff}} \pm \sigma_{\text{Ran}} \pm \sigma_{\text{Sys}}$ [K]	$M_{\star} \pm \sigma_{\text{Ran}} \pm \sigma_{\text{Sys}}$ [M_{\odot}]	$R_{\star} \pm \sigma_{\text{Ran}} \pm \sigma_{\text{Sys}}$ [R_{\odot}]	$R_{\text{P}} \pm \sigma_{\text{Ran}} \pm \sigma_{\text{Sys}}$ [R_{\oplus}]	$T_{\text{eq}} \pm \sigma_{\text{Sys}}$ [K]
1078.01	M1V	-0.26 \pm 0.12 \pm 0.10	3808 $^{+72}_{-58}$ \pm 50	0.33 \pm 0.06 \pm 0.05	0.30 \pm 0.05 \pm 0.04	1.16 \pm 0.18 \pm 0.16	529 \pm 59
430.01	M1V	-0.10 \pm 0.05 \pm 0.10	3799 $^{+53}_{-40}$ \pm 50	0.38 \pm 0.04 \pm 0.04	0.34 \pm 0.03 \pm 0.03	1.45 \pm 0.13 \pm 0.13	356 \pm 28
254.01	M1V	0.20 \pm 0.03 \pm 0.10	3814 $^{+48}_{-48}$ \pm 50	0.46 \pm 0.03 \pm 0.03	0.41 \pm 0.02 \pm 0.02	8.21 \pm 0.48 \pm 0.45	650 \pm 33
1152.01	M1V	-0.13 \pm 0.02 \pm 0.10	3807 $^{+36}_{-27}$ \pm 50	0.38 \pm 0.02 \pm 0.04	0.34 \pm 0.02 \pm 0.03	10.07 \pm 0.60 \pm 0.84	491 \pm 35
1176.01	M1V	-0.06 \pm 0.16 \pm 0.10	3808 $^{+322}_{-142}$ \pm 50	0.40 \pm 0.13 \pm 0.06	0.36 \pm 0.11 \pm 0.05	6.20 \pm 1.85 \pm 0.82	672 \pm 71
251.01	M1V	-0.02 \pm 0.03 \pm 0.10	3813 $^{+44}_{-34}$ \pm 50	0.42 \pm 0.03 \pm 0.05	0.38 \pm 0.02 \pm 0.04	1.84 \pm 0.10 \pm 0.20	530 \pm 47
1266.01	M1V	-0.21 \pm 0.07 \pm 0.10	3825 $^{+169}_{-103}$ \pm 50	0.36 \pm 0.09 \pm 0.04	0.32 \pm 0.07 \pm 0.03	0.92 \pm 0.19 \pm 0.10	361 \pm 31
51.01	M1V	a	3839 $^{+984}_{-227}$ \pm 50 ^a				
248.01	M1V	-0.05 \pm 0.05 \pm 0.10	3819 $^{+67}_{-52}$ \pm 50	0.41 \pm 0.04 \pm 0.04	0.37 \pm 0.03 \pm 0.03	1.60 \pm 0.14 \pm 0.14	440 \pm 33
248.02	1.38 \pm 0.12 \pm 0.12	383 \pm 28
248.03	1.11 \pm 0.10 \pm 0.10	620 \pm 46
868.01	M1V	0.02 \pm 0.05 \pm 0.10	3822 $^{+74}_{-57}$ \pm 50	0.43 \pm 0.04 \pm 0.04	0.39 \pm 0.03 \pm 0.03	6.80 \pm 0.58 \pm 0.58	140 \pm 10
663.01	M1V	-0.25 \pm 0.01 \pm 0.10	3838 $^{+19}_{-19}$ \pm 50	0.36 \pm 0.02 \pm 0.04	0.32 \pm 0.01 \pm 0.03	0.87 \pm 0.03 \pm 0.08	579 \pm 43
663.02	0.78 \pm 0.03 \pm 0.07	298 \pm 22
314.01	M1V	-0.18 \pm 0.00 \pm 0.10	3846 $^{+9}_{-9}$ \pm 50	0.39 \pm 0.01 \pm 0.03	0.35 \pm 0.01 \pm 0.03	1.09 \pm 0.02 \pm 0.09	350 \pm 24
314.02	0.91 \pm 0.02 \pm 0.07	294 \pm 20
875.01	M0V	-0.05 \pm 0.09 \pm 0.10	3861 $^{+173}_{-97}$ \pm 50	0.44 \pm 0.08 \pm 0.05	0.39 \pm 0.06 \pm 0.04	1.91 \pm 0.32 \pm 0.18	540 \pm 43
1427.01	M0V	-0.20 \pm 0.06 \pm 0.10	3880 $^{+119}_{-77}$ \pm 50	0.40 \pm 0.06 \pm 0.04	0.36 \pm 0.05 \pm 0.03	0.80 \pm 0.11 \pm 0.07	622 \pm 45
1596.01	M0V	-0.28 \pm 0.05 \pm 0.10	3882 $^{+134}_{-82}$ \pm 50	0.38 \pm 0.07 \pm 0.04	0.34 \pm 0.06 \pm 0.03	0.78 \pm 0.13 \pm 0.08	462 \pm 37
1596.02	1.19 \pm 0.20 \pm 0.11	177 \pm 14
812.01	M0V	-0.36 \pm 0.06 \pm 0.10	3890 $^{+129}_{-78}$ \pm 50	0.35 \pm 0.07 \pm 0.04	0.31 \pm 0.06 \pm 0.03	1.38 \pm 0.24 \pm 0.15	547 \pm 49
812.02	1.22 \pm 0.22 \pm 0.13	301 \pm 27
812.03	1.16 \pm 0.21 \pm 0.13	228 \pm 20
250.01	M0V	-0.08 \pm 0.05 \pm 0.10	3886 $^{+108}_{-71}$ \pm 50	0.44 \pm 0.05 \pm 0.03	0.39 \pm 0.04 \pm 0.03	2.08 \pm 0.23 \pm 0.15	381 \pm 23
250.02	2.08 \pm 0.23 \pm 0.15	340 \pm 21
250.03	0.75 \pm 0.08 \pm 0.05	577 \pm 36
448.01	M0V	-0.28 \pm 0.04 \pm 0.10	3895 $^{+95}_{-61}$ \pm 50	0.39 \pm 0.05 \pm 0.04	0.35 \pm 0.04 \pm 0.03	1.12 \pm 0.14 \pm 0.10	391 \pm 29
448.02	1.85 \pm 0.23 \pm 0.16	240 \pm 17
898.01	M0V	-0.15 \pm 0.05 \pm 0.10	3894 $^{+112}_{-71}$ \pm 50	0.43 \pm 0.06 \pm 0.03	0.38 \pm 0.05 \pm 0.03	1.68 \pm 0.20 \pm 0.12	408 \pm 26
898.02	1.34 \pm 0.16 \pm 0.10	505 \pm 32
898.03	1.40 \pm 0.17 \pm 0.10	321 \pm 20
877.01	M0V	-0.20 \pm 0.03 \pm 0.10	3897 $^{+96}_{-63}$ \pm 50	0.41 \pm 0.05 \pm 0.03	0.37 \pm 0.04 \pm 0.03	1.36 \pm 0.15 \pm 0.10	478 \pm 30
877.02	1.25 \pm 0.14 \pm 0.09	378 \pm 24
775.01	M0V	-0.09 \pm 0.05 \pm 0.10	3897 $^{+112}_{-69}$ \pm 50	0.45 \pm 0.05 \pm 0.03	0.40 \pm 0.04 \pm 0.03	1.22 \pm 0.13 \pm 0.08	348 \pm 21
775.02	1.46 \pm 0.16 \pm 0.10	445 \pm 26
1588.01	M0V	-0.24 \pm 0.03 \pm 0.10	3916 $^{+66}_{-46}$ \pm 50	0.41 \pm 0.04 \pm 0.03	0.37 \pm 0.03 \pm 0.03	0.87 \pm 0.07 \pm 0.06	572 \pm 36
676.01	M0V	-0.12 \pm 0.02 \pm 0.10	3913 $^{+59}_{-41}$ \pm 50	0.45 \pm 0.03 \pm 0.03	0.40 \pm 0.02 \pm 0.02	2.58 \pm 0.15 \pm 0.15	444 \pm 23
676.02	1.66 \pm 0.10 \pm 0.10	658 \pm 35
1361.01	M0V	-0.02 \pm 0.04 \pm 0.10	3926 $^{+130}_{-79}$ \pm 50	0.48 \pm 0.05 \pm 0.03	0.42 \pm 0.05 \pm 0.03	1.58 \pm 0.17 \pm 0.10	232 \pm 13
1024.01	M0V	-0.27 \pm 0.04 \pm 0.10	3941 $^{+91}_{-66}$ \pm 50	0.42 \pm 0.05 \pm 0.03	0.37 \pm 0.04 \pm 0.03	1.02 \pm 0.11 \pm 0.07	490 \pm 30
1085.01	M0V	-0.25 \pm 0.06 \pm 0.10	3942 $^{+123}_{-87}$ \pm 50	0.43 \pm 0.06 \pm 0.04	0.38 \pm 0.05 \pm 0.03	0.68 \pm 0.09 \pm 0.05	446 \pm 29
1577.01	M0V	-0.18 \pm 0.06 \pm 0.10	3943 $^{+177}_{-102}$ \pm 50	0.45 \pm 0.08 \pm 0.03	0.40 \pm 0.06 \pm 0.03	0.96 \pm 0.16 \pm 0.06	634 \pm 37
1515.01	M0V	-0.36 \pm 0.02 \pm 0.10	3948 $^{+49}_{-46}$ \pm 50	0.40 \pm 0.03 \pm 0.03	0.36 \pm 0.03 \pm 0.03	0.70 \pm 0.05 \pm 0.06	695 \pm 48
605.01	M0V	-0.03 \pm 0.13 \pm 0.10	3939 $^{+124}_{-80}$ \pm 50	0.49 \pm 0.06 \pm 0.04	0.43 \pm 0.05 \pm 0.03	1.29 \pm 0.15 \pm 0.10	664 \pm 45
901.01	M0V	-0.14 \pm 0.06 \pm 0.10	3946 $^{+205}_{-111}$ \pm 50	0.46 \pm 0.08 \pm 0.03	0.41 \pm 0.07 \pm 0.03	3.25 \pm 0.56 \pm 0.21	386 \pm 22
902.01	M0V	-0.37 \pm 0.06 \pm 0.10	3965 $^{+169}_{-105}$ \pm 50	0.41 \pm 0.08 \pm 0.04	0.36 \pm 0.07 \pm 0.04	3.17 \pm 0.60 \pm 0.31	199 \pm 16
1403.01	M0V	-0.20 \pm 0.06 \pm 0.10	4000 $^{+200}_{-200}$ \pm 50 ^b	0.47 \pm 0.11 \pm 0.03	0.42 \pm 0.09 \pm 0.03	1.25 \pm 0.27 \pm 0.08	347 \pm 19

TABLE 1 — *Continued*

KOI	Sp Type	[M/H] $\pm \sigma_{\text{Ran}} \pm \sigma_{\text{Sys}}$	$T_{\text{eff}} \pm \sigma_{\text{Ran}} \pm \sigma_{\text{Sys}}$ [K]	$M_* \pm \sigma_{\text{Ran}} \pm \sigma_{\text{Sys}}$ [M_{\odot}]	$R_* \pm \sigma_{\text{Ran}} \pm \sigma_{\text{Sys}}$ [R_{\odot}]	$R_{\text{P}} \pm \sigma_{\text{Ran}} \pm \sigma_{\text{Sys}}$ [R_{\oplus}]	$T_{\text{eq}} \pm \sigma_{\text{Sys}}$ [K]
156.01	M0V	$-0.20 \pm 0.02 \pm 0.10$	$3984^{+74}_{-59} \pm 50$	$0.46 \pm 0.04 \pm 0.03$	$0.41 \pm 0.03 \pm 0.02$	$1.02 \pm 0.07 \pm 0.05$	456 ± 22
156.02	$0.86 \pm 0.06 \pm 0.05$	527 ± 26
156.03	$1.51 \pm 0.11 \pm 0.08$	401 ± 20
531.01	M0V	$0.10 \pm 0.03 \pm 0.10$	$4047^{+249}_{-131} \pm 50$	$0.56 \pm 0.08 \pm 0.02$	$0.49 \pm 0.07 \pm 0.02$	$3.02 \pm 0.46 \pm 0.12$	639 ± 24
438.01	M0V	$-0.22 \pm 0.04 \pm 0.10$	$3987^{+135}_{-93} \pm 50$	$0.46 \pm 0.06 \pm 0.03$	$0.41 \pm 0.05 \pm 0.02$	$1.31 \pm 0.17 \pm 0.08$	503 ± 26
503.01	M0V	$-0.13 \pm 0.04 \pm 0.10$	$4003^{+143}_{-95} \pm 50$	$0.49 \pm 0.06 \pm 0.03$	$0.43 \pm 0.05 \pm 0.02$	$1.62 \pm 0.19 \pm 0.08$	463 ± 22
1408.01	M0V	$-0.11 \pm 0.03 \pm 0.10$	$4022^{+118}_{-83} \pm 50$	$0.51 \pm 0.05 \pm 0.02$	$0.45 \pm 0.04 \pm 0.02$	$1.07 \pm 0.10 \pm 0.05$	388 ± 17
500.01	M0V	$-0.14 \pm 0.04 \pm 0.10$	$4037^{+141}_{-95} \pm 50$	$0.51 \pm 0.06 \pm 0.03$	$0.44 \pm 0.05 \pm 0.02$	$1.62 \pm 0.18 \pm 0.08$	495 ± 23
500.02	$1.68 \pm 0.19 \pm 0.09$	448 ± 21
500.03	$0.90 \pm 0.10 \pm 0.05$	654 ± 30
500.04	$1.26 \pm 0.14 \pm 0.06$	569 ± 26
500.05	$0.72 \pm 0.08 \pm 0.04$	955 ± 45
1475.01	M0V	$-0.23 \pm 0.08 \pm 0.10$	$4000^{+200}_{-200} \pm 50$ ^b	$0.47 \pm 0.11 \pm 0.04$	$0.41 \pm 0.09 \pm 0.03$	$1.17 \pm 0.26 \pm 0.08$	783 ± 48
1475.02	$1.43 \pm 0.32 \pm 0.10$	433 ± 26
1141.01	M0V	$-0.13 \pm 0.04 \pm 0.10$	$4000^{+200}_{-200} \pm 50$ ^b	$0.49 \pm 0.10 \pm 0.03$	$0.43 \pm 0.09 \pm 0.02$	$1.29 \pm 0.26 \pm 0.07$	521 ± 25
870.01	M0V	$-0.17 \pm 0.04 \pm 0.10$	$4000^{+200}_{-200} \pm 50$ ^b	$0.48 \pm 0.10 \pm 0.03$	$0.42 \pm 0.09 \pm 0.02$	$1.36 \pm 0.28 \pm 0.07$	512 ± 25
870.02	$1.32 \pm 0.27 \pm 0.07$	446 ± 22
222.01	M0V	$-0.17 \pm 0.05 \pm 0.10$	$4000^{+200}_{-200} \pm 50$ ^b	$0.48 \pm 0.11 \pm 0.03$	$0.42 \pm 0.09 \pm 0.02$	$1.53 \pm 0.32 \pm 0.08$	501 ± 25
222.02	$1.24 \pm 0.26 \pm 0.07$	396 ± 19
1584.01	M0V	$-0.32 \pm 0.10 \pm 0.10$	$4000^{+200}_{-200} \pm 50$ ^b	$0.44 \pm 0.11 \pm 0.05$	$0.39 \pm 0.09 \pm 0.04$	$1.03 \pm 0.25 \pm 0.10$	500 ± 41
912.01	M0V	$-0.19 \pm 0.04 \pm 0.10$	$4000^{+200}_{-200} \pm 50$ ^b	$0.47 \pm 0.11 \pm 0.03$	$0.42 \pm 0.09 \pm 0.02$	$1.70 \pm 0.35 \pm 0.10$	417 ± 21
104.01	M0V	$-0.12 \pm 0.01 \pm 0.10$	$4000^{+200}_{-200} \pm 50$ ^b	$0.49 \pm 0.10 \pm 0.03$	$0.43 \pm 0.09 \pm 0.02$	$1.66 \pm 0.33 \pm 0.08$	688 ± 31
1202.01	M0V	$-0.06 \pm 0.06 \pm 0.10$	$4000^{+200}_{-200} \pm 50$ ^b	$0.51 \pm 0.10 \pm 0.03$	$0.45 \pm 0.09 \pm 0.03$	$1.26 \pm 0.25 \pm 0.08$	967 ± 53
1298.01	K7V	$-0.37 \pm 0.12 \pm 0.10$ ^c	$4400^{+200}_{-200} \pm 50$ ^b	$0.60 \pm 0.08 \pm 0.04$	$0.54 \pm 0.07 \pm 0.04$	$2.59 \pm 0.36 \pm 0.18$	498 ± 28
904.01	K7V	$-0.15 \pm 0.11 \pm 0.10$ ^c	$4400^{+200}_{-200} \pm 50$ ^b	$0.64 \pm 0.07 \pm 0.04$	$0.58 \pm 0.07 \pm 0.04$	$1.68 \pm 0.20 \pm 0.10$	870 ± 45
904.02	$2.40 \pm 0.29 \pm 0.15$	373 ± 19
956.01	K7V	$-0.47 \pm 0.06 \pm 0.10$ ^c	$4400^{+200}_{-200} \pm 50$ ^b	$0.58 \pm 0.08 \pm 0.02$	$0.51 \pm 0.07 \pm 0.02$	$2.49 \pm 0.35 \pm 0.11$	537 ± 21
977.01	M1III	^d					

^a The signal-to-noise achieved on KOI 51 was not high enough to measure [M/H].

^b The H₂O-K2 index saturates at temperatures near and above 3900 K. For those objects with unreasonably large T_{eff} errors we chose a T_{eff} based on the spectral type, and ascribe an uncertainty of 200 K.

^c The relation used to obtain [M/H] is calibrated using only M dwarfs. The [M/H] estimates for the K7V objects are an extrapolation to K dwarfs.

^d The [M/H] and T_{eff} for KOI 977 (M1III) could not be determined.